ELSEVIER

Journal of Molecular Graphics and Modelling 21 (2003) 473–486

Journal of Molecular Graphics and Modelling

www.elsevier.com/locate/JMGM

Prediction of the multimeric assembly of staphylococcal enterotoxin A with cell-surface protein receptors

Lilee Cuff [a], Robert G. Ulrich [b], Mark A. Olson [a,*]

[a] *Department of Cell Biology and Biochemistry, USAMRIID, 1425 Porter Street, Frederick, MD 21702, USA*
[b] *Department of Immunology and Molecular Biology, USAMRIID, 1425 Porter Street, Frederick, MD 21702, USA*

Received 16 August 2002; received in revised form 26 November 2002; accepted 26 November 2002

Abstract

Staphylococcal enterotoxin A (SEA) cross-links two class II major histocompatibility complex (MHC) molecules and forms a multimeric assembly with T-cell receptors (TcRs). The X-ray crystal structure of SEA has been solved, yet details describing molecular recognition and association remain unclear. We present a structural model for the interactions of SEA with cell-surface proteins. Molecular docking calculations predicting SEA association with the class II MHC molecule HLA-DR1 were performed by using a rigid-body docking method. Docked orientations were evaluated by a Poisson–Boltzmann model for the electrostatic free energy of binding and the hydrophobic effect calculated from molecular surface areas. We found that the best-scoring SEA conformers for the DR1α interface display a binding mode similar to that determined crystallographically for staphylococcal enterotoxin B bound to HLA-DR1. For the zinc-binding site of SEA, docking DR1β yielded several orientations exhibiting tetrahedral-like coordination geometries. Combining the two interfaces, tetramers were modeled by docking an αβ TcR with trimolecular complexes DR1β–SEA–DR1α and SEA–βDR1α–SEA. Our results indicate that the complex DR1β–SEA–DR1α provides a more favorable assembly for the engagement of TcRs, forming SEA molecular contacts that are in accord with reported mutagenesis studies. In contrast, the cooperative association of two SEA molecules on a single DR1 molecule sterically inhibits interactions with TcRs. We suggest that signal transduction stimulated by SEA through large-scale assembly is limited to four or five TcR–(DR1β–SEA–DR1α) tetramers and requires the dimerization of class II MHC molecules, while TcR dimerization is unlikely. Published by Elsevier Science Inc.

Keywords: Protein docking; Continuum model; Free energy of binding; Protein–protein complex

1. Introduction

The assembly of heterogeneous proteins on cell surfaces for the function of signal transduction is one of the most interesting topics in structural molecular biology. An illustrative example is the superantigens (SAgs), which are viral and bacterial proteins capable of prolific signal transduction of T-cells and antigen-presenting cells. SAgs are presented by glycoproteins of class II major histocompatibility complex (MHC) in a conformational manner that elicits interactions with a broad repertoire of variable β-chain (Vβ) domain elements of T-cell receptors (TcRs) [1,2]. Their ability to overstimulate T-cells is associated with a number of illnesses, including food poisoning and toxic-shock syndrome (for a review, see [3]).

Among the SAgs, the zinc-containing staphylococcal enterotoxin A (SEA) has attracted considerable interest, in particular, conjectures regarding conformational-binding properties. Various studies implicate a requirement that for effective superantigenicity, a single SEA protein must bind simultaneously two class II MHC proteins on antigen-presenting cells [4,5]. Binding of SEA occurs through an interface with the DRα chain of class II MHC molecules and a zinc-coordination site with the DRβ chain. While the X-ray crystal structure of SEA is known [6,7], cocrystal structures with either class II MHC molecules or TcRs remain to be determined. From structural similarity with the cocrystal structure of the monovalent staphylococcal enterotoxin B (SEB) with HLA-DR1 [8] and site-directed mutagenesis data [9], it can be inferred that SEA forms the trimer DR1β–SEA–DR1α using a DR1α binding determinant common with SEB. However, additional experimental data indicate that two SEA molecules can bind to one HLA-DR molecule in solution [10], thus suggesting the SEA–βDR1α–SEA complex for cross-linking DR1, where the notation –βDR1α– denotes both α- and β-binding sites. This latter complex is widely used in the literature as a model for the T-cell response to SEA–DR1 (see, e.g. [5,11]). Yet, from experimental studies, it is not clear as

* Corresponding author. Tel.: +1-301-619-4236; fax: +1-301-619-2348.
E-mail address: molson@ncifcrf.gov (M.A. Olson).

1093-3263/03/$ – see front matter. Published by Elsevier Science Inc.
doi:10.1016/S1093-3263(02)00206-1

to what type of multimeric complex configurations on cell surfaces favors SEA engagement of TcRs, and under what structural conditions permit the large-scale assembly that is thought to enhance the delivering of activation signals [12].

To learn more about the mechanism of molecular recognition and binding of SEA, molecular docking calculations with HLA-DR1 and a modeled αβ TcR were performed. For predicting the DR1α and DR1β interfaces, a protein–protein docking method [13,14] was used for matching SEA and DR1 complementary surfaces by rigid-body sampling of orientational space. Unlike the inherent assumption of constraining similarity in comparative modeling of SEA complex formation using the SEB–DR1 complex [9,12], molecular docking simulates the recognition process and allows for an assessment of the importance of shape and electrostatic complementarity. Scoring the generated complex configurations was based on a continuum model of the total electrostatic free energy contribution to molecular association, evaluated using the finite-difference Poisson–Boltzmann (FDPB) method. Non-polar contributions were estimated by employing an interfacial free energy term derived from molecular surface areas.

The combination of docking and the semi-macroscopic evaluation of binding free energies has been applied with success [15] to reconstituting the SEB–DR1 crystallographic complex. Similarly, these methods were able to accurately discriminate between native-like and non-native docked configurations of the poorly resolved cocrystal structure of toxic-shock syndrome toxin with HLA-DR1 [16]. Here, in addition to predicting the global orientation of bound SEA, we also used continuum methods to calculate the binding 'signature' for the SEA–DR1α interface. This computational approach provides an efficient framework of elucidating structural and thermodynamic correlates that govern the nature of binding and of locating critical-binding sites for protein assemblies. A similar calculated signature for SEB is presented from the previous docking of the DR1 complex, and when compared with SEA, new insight is obtained into possible association pathways of SAgs.

Because of the lack of an αβ TcR tertiary structure that interacts with SEA, oligomers for Vβ using a sequence that interacts with SEA were constructed by homology from the cocrystal structure of SEC3 complexed with the β-chain of a TcR [17]. Docking this model and its correspondence to known experimental biochemical results allows a better understanding of the interaction of SEA with TcRs.

2. Methods

2.1. Protein–protein docking

The tertiary structures for SEA (PDB:1esf) and HLA-DR1 (PDB:1seb) employed in the molecular docking calculations are illustrated in Fig. 1. For calculating the protein–protein interface stabilized by possible sidechain reorientations, a strategy of sampling configurational space was implemented by using the native and a modified SEA structure. Sidechain reorientations at two SEA contact regions were assumed to adopt the geometry of the bound SEB conformation with DR1α. These contact surfaces are designated as the 'hydrophobic loop' and 'polar pocket' interfacial regions. The hydrophobic loop connects strands β_1 and β_2 of the protein fold, and consists of residues Gln46, Phe47, and Leu48 (Fig. 1a). The polar pocket is derived from three β strands of the β-barrel domain, and contains residues Asp70, Tyr92, and Tyr108. Both regions are structurally conserved

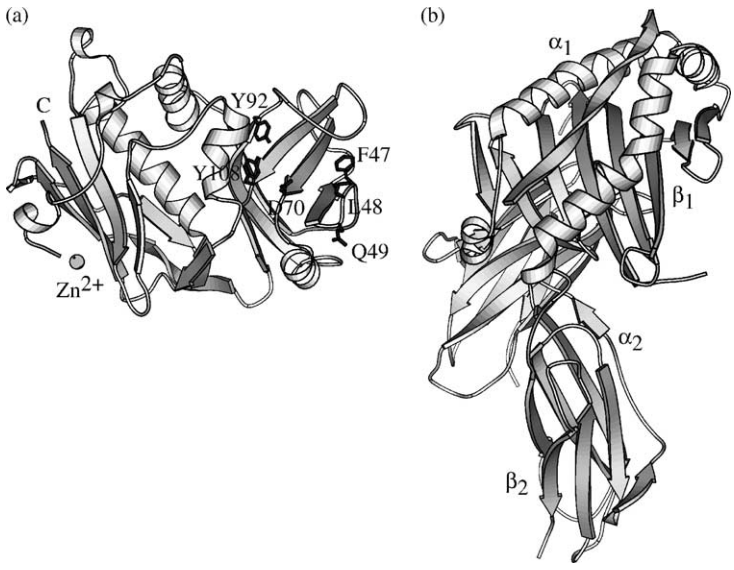

Fig. 1. Tertiary structures for the superantigen SEA (a) and the human class II MHC molecule HLA-DR1 (b). Several key residues are highlighted for SEA. The HLA-DR1 receptor consists of an αβ heterodimer each containing two structural domains (α_1, α_2; β_1, β_2).

among the reported crystal structures of staphylococcal enterotoxins.

Multiple-docked orientations for SEA were generated by rigid-body conformational sampling and energy minimization method implemented in the program DOCK [13,14]. SEA–DR1α shape complementarity was achieved by matching clusters of spheres generated from a SEA molecular surface formed by residues within 5.0 Å radius from Leu48 of hydrophobic loop region and an equivalent radius from Asp70 of the polar pocket. Because of the size of the DR1 molecule, only the α_1 chain (residues 1–80) was used in docking calculations of the α-binding mode. The corresponding DR1α_1 surface included residues within a 5.0 Å radius from residues Gln18 and Lys39. Molecular surfaces were generated by the MS program [18], using a solvent probe of radius 1.4 Å. The number of spheres was set at 48 for SEA and 153 for DR1α_1. The bin width, overlap, and distance-matching tolerance were set to values of 1.0, 0.5, and 1.5 Å, respectively. The number of bad contacts was limited to five and the molecular contact score set a 120. Force-field scores were calculated by using the AMBER potential function [19], and DR1α_1 orientations with energies less than −20.0 kcal/mol were analyzed by the continuum method.

For docking the SEA zinc-coordination site with DR1β, calculations were carried out by using the β_1 chain (DR1β_1) together with residues 50–58 of DR1α_1 and residues 1–4 of the polyalanine antigenic peptide. The chelating water molecule was removed before docking and residues 1–6 of the N-terminus were truncated to open up the zinc cavity. The SEA interfacial surface was defined as consisting of residues within a 5.0 Å radius from the zinc ion, and the DR1β_1 surface from residue His81. The number of spheres for SEA was set at 27 and 68 for DR1. Parameters for Zn^{2+} were taken from Hoops et al. [20] and implemented in the AMBER force field. Minimum molecular contact score and potential energy were set at values corresponding to 100 and −10.0 kcal/mol, respectively. A molecular dynamics (MD) simulated annealing method was applied for repositioning residues 1–20 of the docked configurations. All MD simulations treated non-bonded interactions with a cutoff radius of 12.0 Å and modeled solvent effects implicitly by using a distance-dependent dielectric of $\varepsilon = 2r$. The integration timestep was set at 1.0 fs. MD calculations were initiated with 200 cycles of energy minimization by using a conjugate gradient method, followed by a simulation for 500 steps at a temperature of 1000 K. This was then followed by an annealing protocol for a temperature range of 250–1000 K, employing an interval of 25 K from the initial high temperature. Each simulation was completed for 1000 steps and started from the previous temperature by using the final calculated structure. Backbone angle restraints of 100 kcal/mol rad^2 were placed on residues 4–7 during annealing, preserving the one-turn helix. The lowest-energy conformer was taken as the final predicted structure.

Using the Vβ3 amino acid sequence [21], a comparative model for the Vβ domain of a TcR was constructed from the cocrystal structure of the extracellular portion of Vβ8.2 complexed with SEC3 [18]. This homology structure was docked with SEA. Spheres were modeled for Vβ3 residues located within a 3 Å distance from SEA, as superposed on the SEC cocrystal structure. The contact surface for Vβ3 contained 99 spheres. Interfacial residues for SEA were taken from 4 Å away from Vβ3 and resulted in 44 spheres. Docking parameters were set at a bin width, overlap, and distance-matching tolerance of 1.5, 1.5 and 1.0 Å, respectively. The number of bad contacts was limited to three and the molecular contact score set a 150 with a maximum force-field score of −15 kcal/mol. The structure for Vα was obtained from the crystallographic structure of an αβ TcR bound to the human class I MHC HLA-A2 molecule [22].

2.2. Continuum model

The molecular association of SEA (denoted as P) with either the α- or β-chain of HLA-DR1 (L) can be described as a two-step process (see, e.g. [23])

$$\mathrm{P} + \mathrm{L} \overset{\Delta G_{\mathrm{conf}}}{\rightleftharpoons} \mathrm{P}^* + \mathrm{L}^*, \tag{1}$$

$$\mathrm{P}^* + \mathrm{L}^* \overset{\Delta G_{\mathrm{static}}}{\rightleftharpoons} \mathrm{P}^*\mathrm{L}^*, \tag{2}$$

where the first step accounts for the conformational change from the native P and L conformers to the functional conformers P* and L*, and the second step describes the binding of the two molecules in their functional state. The Gibbs free energy of binding is obtained by combining Eqs. (1) and (2)

$$\begin{aligned}\Delta G_{\mathrm{bind}} &= \Delta G_{\mathrm{conf}} + \Delta G_{\mathrm{static}} \\ &= \Delta G_{\mathrm{conf}} + \Delta W + \Delta G_{\mathrm{int}} - T\Delta S,\end{aligned} \tag{3}$$

where ΔG_{conf} is the free energy shift upon conformational changes and $\Delta G_{\mathrm{static}}$ is the non-relaxation free energy. Here, we will focus primarily on $\Delta G_{\mathrm{static}}$ and partition the free energy into independent energetic contributions, where ΔW represents the change in solute–solvent interactions for P* and L* due to binding, ΔG_{int} is the interaction free energy between the bound molecules, and $T\Delta S$ is the change in non-electrostatic entropy determined at temperature T.Contained in Eq. (3), we define our scoring function for docked complex configurations as a microscopic state (conformer) free energy given by $\Delta G_{\mathrm{micro}} = \Delta W + \Delta G_{\mathrm{int}}$. Theoretical models describing ΔW are based on the following formalism of separating the term:

$$\Delta W = \Delta G_{\mathrm{cav}} + \Delta G_{\mathrm{s,vdW}} + \Delta G_{\mathrm{s,ele}}, \tag{4}$$

where ΔG_{cav} is the change in free energy required to form the solute-sized cavities in the solvent, $\Delta G_{\mathrm{s,vdW}}$ is the free energy change in van der Waals (vdW) interactions of inserting solute molecules into the cavities, and $\Delta G_{\mathrm{s,ele}}$ is the

change in the free energy of solvent polarization. The cavitation term models the hydrophobic effect and is proportional to the change in solvent-exposed surface area upon association with a constant surface tension, γ,

$$\Delta G_{\text{cav}} = \gamma(A_{\text{P*L*}} - A_{\text{P*}} - A_{\text{L*}}), \tag{5}$$

where the As denote either molecular surface areas or solvent-accessible surface areas. We selected to apply molecular surfaces determined by the MS algorithm [18] with the solvent probe radius set at 1.4 Å and the value of the proportionality constant γ set at 69 cal/mol/Å [24].

The contribution ΔG_{int} contains polar and non-polar intermolecular interaction terms between P* and L*

$$\Delta G_{\text{int}} = \Delta G_{\text{m,vdW}} + \Delta G_{\text{m,ele}}, \tag{6}$$

where $\Delta G_{\text{m,vdW}}$ is the van der Waals contribution and $\Delta G_{\text{m,ele}}$ the electrostatic interaction component. The term $\Delta G_{\text{m,vdW}}$ combined with $\Delta G_{\text{s,vdW}}$ of Eq. (4) may be neglected as an approximation by invoking an enthalpy–entropy compensation phenomenon argument [25].

The electrostatic free energies given in Eqs. (4) and (6) can be conveniently calculated from a thermodynamic process of charging and uncharging P* and L* on complex formation (see, e.g. [26,27])

$$\begin{aligned}\Delta G_{\text{ele}} &= \int_V [(\rho^{\text{P*L*}'}\varphi^{\text{P*L*}'} - \rho^{\text{P*}}\varphi^{\text{P*}}) \\ &\quad + (\rho^{\text{P*}'\text{L*}}\varphi^{\text{P*}'\text{L*}} - \rho^{\text{L*}}\varphi^{\text{L*}}) + \rho^{\text{P*}}\varphi^{\text{L*}}]\,\mathrm{d}\boldsymbol{r} \\ &= \Delta\Delta G^{\text{P*L*}'}_{\text{s,ele}} + \Delta\Delta G^{\text{P*}'\text{L*}}_{\text{s,ele}} + \Delta G^{\text{P*L*}}_{\text{m,ele}},\end{aligned} \tag{7}$$

where ρ and φ are the spatially dependent charge density and electrical potential, respectively, in volume element $\mathrm{d}\boldsymbol{r}$. The first term represents the loss of solute–solvent interaction energy through the partial desolvation of the electrostatically charged P* on binding the uncharged L* (denoted as L*′), and similarly, the second term corresponds to the desolvation of L* on binding P*′; the third term is the electrostatic interaction energy between P* and L* in the solvent dielectric.

We applied a FDPB method implemented in the program DelPhi [26] for conformations extracted from docking. The electrostatic potentials for each molecule were calculated by using the solvent-accessible surfaces to define regions of low dielectric medium embedded in a high dielectric solvent water of ionic strength set at 0.145 M. DelPhi calculations were carried out on a cubic grid of resolution set a 1.6 grid points/Å. Numerical error in the calculated electrostatic contribution was approximately 2%, as determined from using a finer grid resolution. The protein dielectric constant was set at $\varepsilon_{\text{p}} = 2$ and a dielectric of 80 was used to model bulk water. Atomic charges and radii parameters were similar to those used in docking. Boundary conditions were set at full coulombic for all calculations. Dummy atoms were implemented for the unbound structures in retaining an identical scale and position on the grid used with the complex configuration.

In the continuum dielectric calculations, the zinc ion was retained explicitly as part of the protein, while crystallographic waters were deleted. The computational success of this approach in evaluating free energies of solvation is system dependent and appears sensitive to molecular surface curvature of the zinc ion site. For example, recent calculations of a zinc protease bound with its peptide substrate and modeling explicitly the ion and coordinated water in the active site cavity reported good qualitative agreement with the experimental free energy of Michaelis complex formation [28]. In contrast, incorporating interfacial ions and crystallographic waters into continuum modeling of antibody–antibody binding demonstrated poor results with experimental free energies [29]. The latter is presumably due to a relatively flat interfacial surface common among protein–protein assemblies.

The free energy of binding P* and L* is a collection of many contributions from functional groups (FGs) creating a binding ‘signature’. These FGs encompass sidechains and backbone atoms, and from the process of association, some FGs are unaffected by the process, while others are only partially or completely affected. We modeled only the FGs of P* at the residue sidechain level and denote them as $R_1, R_2, R_3, \ldots, R_M$. A thermodynamic cycle is required such that the sum of individual FG contributions equals the total free energy of complex formation. Given a large number of FGs, one can create various cycles that yield the same free energy, but different FG contributions. Here, the simplest cycle is that of switching a FG on and off one at a time. This allows the electrostatic terms to be conveniently calculated by using a charging and uncharging cycle of turning atomic charges on and off per FG, and is defined as

$$\begin{aligned}\Delta\Delta G^{\text{P*L*}'}_{\text{s,ele}} &= \sum_i^M \Delta\Delta G^{\text{P*L*}'}_{\text{s,ele}} \\ &\quad \times (R'_1, R'_2, \ldots, R_i, R'_{i+1}, \ldots, R'_M; \text{L*}'),\end{aligned} \tag{8}$$

and

$$\begin{aligned}\Delta G^{\text{P*L*}}_{\text{m,ele}} &= \sum_i^M \Delta G^{\text{P*L*}}_{\text{m,ele}} \\ &\quad \times (R'_1, R'_2, \ldots, R_i, R'_{i+1}, \ldots, R'_M; \text{L*}'),\end{aligned} \tag{9}$$

where for the ith term R_i is charged, while the remaining FGs are uncharged. The solvent cavitation energy is similarly decomposed on a per FG buried molecular surface area

$$\Delta G_{\text{cav}} = \gamma \sum_i^M \Delta A_i. \tag{10}$$

The free energy of complex formation can be further decomposed in terms of electrostatic pair interactions (see, e.g. [30])

$$\Delta G^{-+}_{\text{m,ele}} = \Delta G_{\text{pair}} + \Delta G^{-}_{\text{m,ele}} + \Delta G^{+}_{\text{m,ele}}, \tag{11}$$

$$\Delta\Delta G^{-+}_{\text{s,ele}} = \Delta\Delta G^{-}_{\text{s,ele}} + \Delta\Delta G^{+}_{\text{s,ele}}, \tag{12}$$

and

$$\Delta G_{ele}^{-+} = \Delta G_{m,ele}^{-+} + \Delta\Delta G_{s,ele}^{-+}, \quad (13)$$

where ΔG_{pair} defines the electrostatic free energy of pair interaction between bridging sidechains of SEA and DR1α; $\Delta G_{m,ele}^{-}$ is the free energy due to electrostatic interaction between the SEA (negatively charged or neutral) bridging sidechain and non-bridging DR1α residues, and similarly $\Delta G_{m,ele}^{+}$ is for the positively charged sidechain on DR1α. The corresponding desolvation costs are $\Delta\Delta G_{s,ele}^{-}$ and $\Delta\Delta G_{s,ele}^{+}$ for the individual sidechains. The sum of protein interaction and solvation terms are give by, $\Delta G_{m,ele}^{-+}$ and $\Delta\Delta G_{s,ele}^{-+}$.

3. Results and discussion

3.1. SEA–DR1α docking

The total number of predicted bound orientations of native and modified SEA structures was roughly 61 million, with 955 conformers satisfying the initial docking scoring criteria (see Section 2). Fig. 2 presents a plot of the root mean square deviation (RMSD) for assorted docked complex configurations from a SEA orientation obtained by structural alignment on the SEB–DR1 cocrystal structure versus ΔG_{micro} scoring. Calculated free energy terms to ΔG_{micro} are listed in Table 1.

The highest ranked complex obtained has an RMSD of 3.10 Å and exhibits a $\Delta G_{micro} = -19$ kcal/mol, which is nearly 21 kcal/mol more favorable than the next higher energy native conformer. The significance of this large energy gap among conformers is its relationship to molecular specificity [31]. Docking achieves the energy gap by a rigid-body minimum in the total electrostatic free energy contribution to association with DR1. Discrimination among different configurations takes place on an electrostatic free energy surface that is unfavorable, and the configurational sampling searches this surface for the minimum, net electrostatic penalty. Despite the importance of the hydrophobic effect in the protein-docking process, hydrophobicity contributes little to conformational specificity. Notably, the best-scoring orientation exhibits a buried molecular surface area comparable to several other conformers containing significantly less favorable ΔG_{micro}.

We find that docking the DR1α surface complementary to the native SEA hydrophobic loop and polar pocket regions provides sufficient interfacial contacts for the generation of conformers exhibiting SEB-like association modes. In contrast, docking using partitioned DR1α surfaces complementary only to either one of the two SEA regions fails to generate similar favorable complex configurations. This failure of matching disconnected surface clusters for either region is due to a lack of minimal topology and molecular interactions required by the DR1 receptor for recognition. The SEA requisite surface differs from docking studies [15] of the bound SEB conformer, which found that while the polar pocket is important, the hydrophobic loop when combined with the disulfide-bonded loop is sufficient for reconstituting near-native orientations. As described further below, the SEB buried molecular surface area is much greater than that of SEA and is attributed to several key recognition and binding elements located in the variably

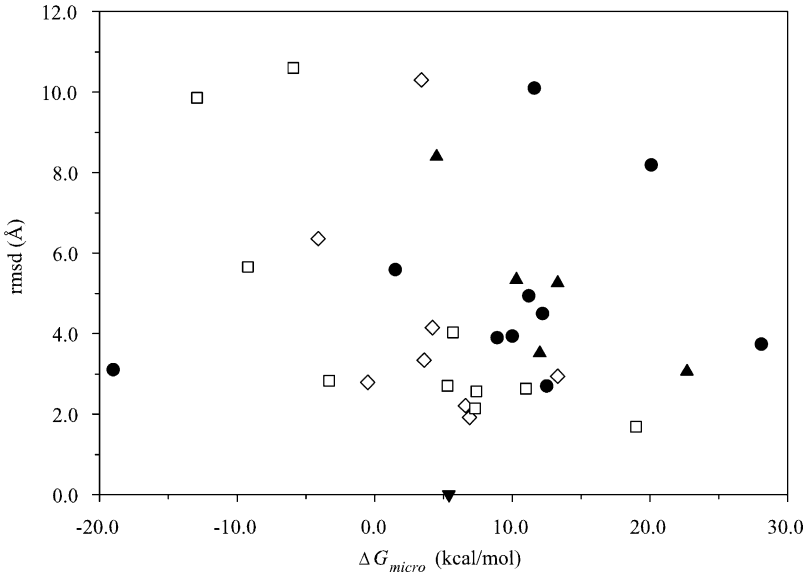

Fig. 2. Free energy scoring versus root mean square deviation (RMSD). Values for RMSD are calculated from the SEA orientation superimposed (via structural alignment) with SEB–DR1 cocrystal structure. Symbols are as follows: (●) native sidechain orientation (docking hydrophobic loop and polar pocket regions); (▲) native sidechain orientation (docking only polar pocket); (□) sidechain reorientation of D70, Y92, Q46, F47 and L48 (docking hydrophobic loop and polar pocket regions); (◇) sidechain reorientation of Q46, F47 and L48 (docking hydrophobic loop and polar pocket regions); (▼) SEA orientation homologous with SEB–DR1 complex configuration.

Table 1
Summary for computed free energies (kcal/mol)

RMSD (Å)	$\Delta\Delta G^{P^*L^{*'}}_{s,ele}$	$\Delta\Delta G^{P^{*'}L^*}_{s,ele}$	$\Delta G^{P^*L^*}_{m,ele}$	ΔG_{ele}	ΔG_{cav}	ΔG_{micro}
SEB equivalent orientation						
0.00	40.5	52.7	−35.2	58.0	−52.6	5.4
Native sidechain orientation (docking hydrophobic loop and polar pocket regions)						
2.70	34.4	35.7	−17.3	52.8	−40.3	12.5
3.10	19.8	39.3	−29.2	29.9	−48.9	−19.0
3.74	38.5	44.8	−12.3	71.0	−42.9	28.1
3.90	43.8	39.0	−23.5	59.3	−50.4	8.9
3.94	36.4	51.8	−28.8	59.4	−49.4	10.0
4.50	21.3	51.5	−18.9	53.9	−41.7	12.2
4.94	25.8	51.3	−19.3	57.8	−46.6	11.2
5.59	26.4	42.6	−26.3	42.7	−41.2	1.5
8.19	31.8	45.7	−12.1	65.4	−45.3	20.1
10.10	24.2	29.1	−15.9	37.4	−25.8	11.6
Native sidechain orientation (docking only polar pocket)						
3.06	43.8	40.0	−21.2	62.6	−39.9	22.7
3.52	40.9	35.8	−21.0	55.7	−43.5	12.0
5.26	35.4	31.6	−18.3	48.7	−35.4	13.3
5.34	31.4	31.2	−18.5	44.1	−33.8	10.3
8.40	23.4	33.3	−16.1	40.6	−36.1	4.5
Native sidechain orientation (docking only hydrophobic loop region)						
40.80	20.7	28.8	2.6	52.1	−31.0	21.1
Sidechain reorientation of D70, Y92, Q46, F47 and L48						
1.92	43.9	28.1	−21.3	50.7	−43.8	6.9
2.21	30.8	38.2	−19.8	49.2	−42.6	6.6
2.79	25.8	31.0	−17.3	39.5	−40.0	−0.5
2.94	33.4	40.1	−19.8	53.7	−40.4	13.3
3.34	29.9	27.1	−17.4	39.6	−36.0	3.6
4.15	24.5	48.6	−22.3	50.8	−46.6	4.2
6.36	26.9	18.6	−13.7	31.8	−35.9	−4.1
10.30	26.5	32.5	−20.8	38.2	−34.8	3.4
Sidechain reorientation of Q46, F47 and L48						
1.69	49.8	40.0	−20.7	69.1	−50.1	19.0
2.14	37.8	36.9	−19.2	55.5	−48.2	7.3
2.57	43.0	26.1	−18.1	51.0	−43.6	7.4
2.64	44.1	24.2	−16.7	51.6	−40.6	11.0
2.70	40.5	23.3	−17.9	45.9	−40.6	5.3
2.83	31.8	26.5	−19.2	39.1	−42.4	−3.3
4.03	30.6	34.8	−19.3	46.1	−40.4	5.7
5.66	25.3	31.1	−20.2	36.2	−45.4	−9.2
9.86	14.7	24.1	−18.8	20.0	−32.9	−12.9
10.60	25.2	22.3	−20.1	27.4	−33.3	−5.9

structured, disulfide-bonded loop region, which are missing in the SEA protein fold.

From Fig. 2, a lower RMSD is found at 2.70 Å, yet requires a significant increase in the free energy of complex formation, showing $\Delta G_{micro} = 12.5$ kcal/mol. Although an allowance of five bad contacts was implemented for docking and scoring, the SEA reference orientation ($\Delta G_{micro} = 5.4$ kcal/mol) is not accessible to docking due to severe steric clashes, yielding a vdW energy four orders of magnitude greater than any of the docked conformers. Relaxing internal degrees of freedom at the interface of this particular orientation by either energy minimization or molecular dynamics clearly does not solve the problem. Thus, by comparison with comparative modeling studies [9,12], the use of molecular docking to search both shape and electrostatic complementarity of the interacting surfaces finds a favorable alternative conformer accounting for structural differences between SEA and SEB. Extracted from the orientational ensemble are several SEA conformations presented in Fig. 3a, illustrating the structural displacements underlying the free energies. Shown for DR1 is the α_1 and β_1 domains bound with the peptide.

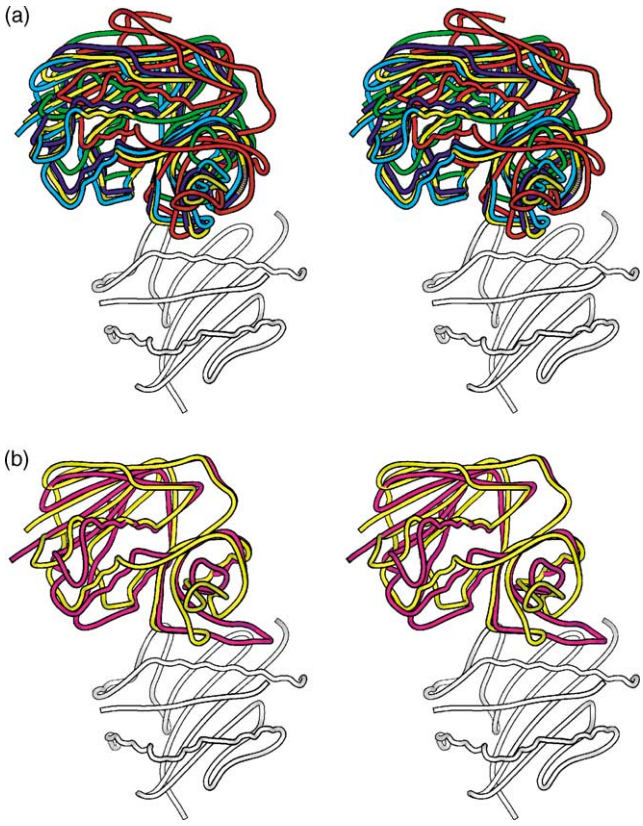

Fig. 3. (a) Stereographic illustration of docked SEA complex configurations with DR1α. The most favorable SEA conformer is colored yellow, while the least favorable is shown in red. DR1 structure is that corresponding to an α_1 and β_1 domains bound with the antigenic peptide. (b) Comparison between the predicted SEA complex configuration (yellow) and the most favorable SEB orientation (magenta) taken from a previous molecular docking study of superantigens [15].

Reorienting the sidechains in either the polar pocket or hydrophobic loop stabilizes the generation of conformers exhibiting greater similarity with SEB–DR1 association (e.g. RMSD of 1.92 Å); however, these orientations incur large penalties in their values of ΔG_{micro} (Fig. 2 and Table 1). This implies that for SEA binding, a structural transition $P \rightarrow P^*$ maximizing surface burial and interaction energy may depend on conformational re-orientations either dissimilar to SEB and/or regions other than the two examined, plus possible changes in the DR1 conformation not found in binding SEB. A comparison of the predicted SEA binding and the X-ray crystal structure for the SEB–DR1 complex is shown in Fig. 3b. The disulfide-bonded loop in SEB

(Cys93–Cys113) is much longer than SEA (Cys96–Cys106) and extends out forming several contacts with the DR1α_1 domain.

While we have obtained a binding mode for SEA–DR1α, the calculation of an absolute binding free energy that is in accord with experiment is a difficult goal. This is particularly true for protein–protein complexes constructed from unbound conformer docking, where atomic complementarity is much less apparent than that of the bound conformations. Further complications arise from the use of moderately resolved crystallographic coordinates. Employing the top-scoring conformer, the free energy of binding can be estimated if we assume theoretical values between 7 and 15 kcal/mol for the rotational and translational entropy loss on complex formation (see, e.g. [32] and references cited therein). Adding the entropic contribution of approximately 10 kcal/mol yields the free energy of association near −9 kcal/mol. The corresponding experimental value is estimated to be −7 kcal/mol for binding DR1α in free solution [4], and thus our model for SEA complex formation appears to capture the correct physics of binding. The precision of the SEA calculations can be further assessed by a comparison with the most favorable SEB–DR1α docked configuration [15] ($\Delta G_{\text{micro}} = -23$ kcal/mol), consequently suggesting a weaker SEA affinity, which is in accordance with the experimental binding free energy of −8 to −10 kcal/mol for SEB [33]. Other researchers employing similar continuum models with $\varepsilon_p = 2$ for macromolecular complexes have found absolute errors in estimating binding free energies ranging from 3 to 49 kcal/mol for orientations extracted from unbound conformer docking of three protease protein–protein inhibitor complexes [34]. Analysis of native crystal complexes indicates errors of 1–20 kcal/mol for the protease complexes [34], and a study of class I MHC protein–peptide interactions reports large errors [35].

One of the adjustable parameters in ΔG_{micro} is the assumed protein 'dielectric constant', which represents all of the electrostatic contributions that are not treated explicitly, rather than a true physical dielectric constant [36,37]. A value of ε_p set at 2, models at the implicit level the induced protein dipoles, while dipolar reorganization from conformational changes upon binding is to be taken into account explicitly. With this approach, the determination of ΔG_{conf} for $\mathsf{P} \rightarrow \mathsf{P}^*$ is required and must have a value less than the free energy of unfolding. Reorganization free energies can be evaluated from all-atom simulations [23,27,38], yet the calculations become computationally prohibitive for large protein–protein assemblies. From the docking calculations, ΔG_{conf} may be marginal and if we take a value of 5 kcal/mol as an upper bound, then ΔG_{bind} is in the range of −4 and −9 kcal/mol. Alternatively, an implicit model can be invoked for ΔG_{conf} by applying $\varepsilon_p = 4$, which embeds reorganization into the $\Delta\Delta G_{\text{s,ele}}$ and $\Delta G_{\text{m,ele}}$ terms. This continuum treatment is more common for modeling the effects of amino acid substitutions on complex stabilization, rather than the absolute free energy of binding [39]. Calculations using ε_p set at 4 show a significant increase in the error with experiment, thus supporting the application of smaller values for ε_p.

3.2. SEA–DR1α binding signature

The calculated ΔG_{micro} reflects an aggregate of many contributions at the binding interface, which can be decomposed into individual contributions arising from SEA residues. Table 2 summarizes the calculated key residue contributions (ΔG_{res}), grouped into three structural regions, plus a fourth group termed others. The structural regions contain the hydrophobic loop, polar pocket and the disulfide-bonded loop. Fig. 4 depicts a projection of the sidechain contributions onto the SEA molecular surface. Residues colored red contribute significantly to DR1α association, whereas blue colored residues destabilize the receptor. For comparison purposes, we have included a similar calculation for SEB bound to DR1.

Clear distinction is observed between the binding determinants of SEA and SEB from the cavitation energies (SEA $\Delta G_{\text{cav}} \cong -49$ kcal/mol versus SEB $\Delta G_{\text{cav}} \cong -100$ kcal/mol), yet each is strongly influenced by the shape complementarity of the hydrophobic loop region. Upon binding, this SAg-DR1α interface mimics a typical cross section through a globular protein with low desolvation penalty on folding. Conserved SEA residues Phe47 and Leu48 combine to provide a ΔG_{cav} of roughly 8 kcal/mol that is likely to drive the hydrophobic effect governing molecular association. SEB residues similarly provide significant stabilization. From biochemical experiments, substitution of alanines for SEA Phe47 and Leu48 weaken substantially binding to class II MHC proteins [4,40]. The continuum model indicates that the reduction in binding of these two mutants is a result of the lost in compactness of the interface, while a second-order effect is the lost in sidechain entropy. The hydrophobic loop region contains non-conserved interactions flanking the phenylalanine and leucine. The predicted $\Delta G_{\text{m,ele}}$ of SEA Gln46 plus its ΔG_{cav} compensate for the lack of a large aromatic sidechain positioned at Gln49, where in SEB the tyrosine extends the hydrophobic patch of buried residues.

A second region where hydrophobicity plays a contributory role is the disulfide-bonded loop region. Sequence and structural similarity between the two SAgs in this region is very low. For the SEB disulfide loop, the total interfacial free energy is comparable to that of the hydrophobic loop interface (−13.9 versus −14.4 kcal/mol), and as noted above, successful docking [15] of SEB requires several recognition elements of the loop structure; namely, residues Ile102 and Ser104. Both residues along with His105 provide considerable contacts for ΔG_{cav}, which are missing in SEA. The two polar sidechains also contain significant $\Delta G_{\text{m,ele}}$ contributions, although only Ser104 can overcome its desolvation cost. For SEA, the hydrophobic contact site is Ala97, which is replaced in SEB by a tyrosine. Mutating SEA Ala97 to

Table 2
Residue-level decomposition of SEA and SEB free energy of binding (kcal/mol) with DR1α

Residue SEA (SEB)	$\Delta\Delta G^{P^*L^{*'}}_{s,ele}$	$\Delta G^{P^*L^*}_{m,ele}$	ΔG_{ele}	ΔG_{cav}	ΔG_{res}
Hydrophobic loop region					
Q46 (Q43)	1.1 (0.6)	−3.1 (1.0)	−2.0 (1.6)	−1.5 (−0.9)	−3.5 (0.7)
F47 (F44)	0.7 (0.5)	−0.3 (1.3)	0.4 (1.8)	−5.0 (−5.1)	−4.6 (−3.3)
L48 (L45)	0.0 (0.6)	0.1 (−0.3)	0.1 (0.5)	−3.2 (−4.0)	−3.1 (−3.5)
Q49 (Y46)	0.1 (0.3)	−0.3 (−0.8)	−0.2 (−0.5)	−1.4 (−3.2)	−1.6 (−3.7)
H50 (F47)	1.6 (0.5)	0.3 (−0.2)	1.9 (0.3)	−0.8 (−1.2)	1.1 (−0.9)
Polar pocket region					
D70 (E67)	5.5 (15.1)	−11.7 (31.0)	−6.2 (−15.9)	−0.6 (−1.2)	−6.8 (−17.1)
Y92 (Y89)	0.5 (0.5)	−1.3 (2.5)	−0.8 (−2.0)	−0.6 (−0.7)	−1.4 (−2.7)
Y108 (Y115)	0.9 (1.3)	−1.6 (6.7)	−0.7 (−5.4)	−0.6 (−1.0)	−1.3 (−6.4)
Disulfide loop region					
C96 (C93)	0.0 (0.0)	0.0 (0.0)	0.0 (0.3)	−0.1 (0.0)	−0.1 (0.0)
A97 (Y94)	0.0 (0.8)	−0.1 (0.4)	−0.1 (1.2)	−1.4 (−4.4)	−1.5 (−3.2)
G98 (Q106)	0.1 (0.1)	−0.1 (0.8)	0.1 (0.9)	0.7 (0.0)	−0.7 (1.8)
– (I102)	(0.1)	(0.0)	(0.1)	(−4.6)	(−4.5)
– (S104)	(1.3)	(−6.4)	(−5.1)	(−1.5)	(−6.6)
– (H105)	(4.3)	(−3.6)	(0.7)	(−3.4)	(−2.7)
Others					
Q95 (Q92)	1.4 (1.7)	−1.8 (2.0)	−0.4 (−0.3)	−2.3 (−2.6)	−2.7 (−2.9)
N207 (S211)	1.8 (1.2)	0.9 (2.2)	2.7 (−1.0)	−0.9 (−1.0)	1.8 (−2.0)
R211 (M215)	2.4 (0.3)	−3.3 (0.2)	−0.9 (0.1)	0.2 (−1.4)	−0.7 (−1.3)
R214 (N218)	2.7 (0.4)	0.1 (0.2)	2.8 (0.6)	−0.6 (−0.3)	2.2 (0.3)

tyrosine and SEB Tyr94 to alanine both disrupt DR1 binding [9]. The modeled complexes suggest that the disruption in SEA is due to steric hindrance, and in the case of SEB, the lost in hydrophobic interaction. Proximate to the disulfide loop are conserved residues Gln95 in SEA and Gln92 in SEB (listed as others in Table 2), showing very similar components to ΔG_{res}, suggesting a degree of confidence in the docked SEA complex.

While the shape complementarity for SEA association with DR1α is driven predominately by the hydrophobic loop region, conformational specificity is conferred through the high electrostatic complementarity of the polar pocket. As shown in Table 2, the principal interaction of this region for SEA is the salt bridge between Asp70 and DRα$_1$ Lys39. The equivalent interaction for SEB is much stronger due to the longer sidechain of Glu67. There are two conserved

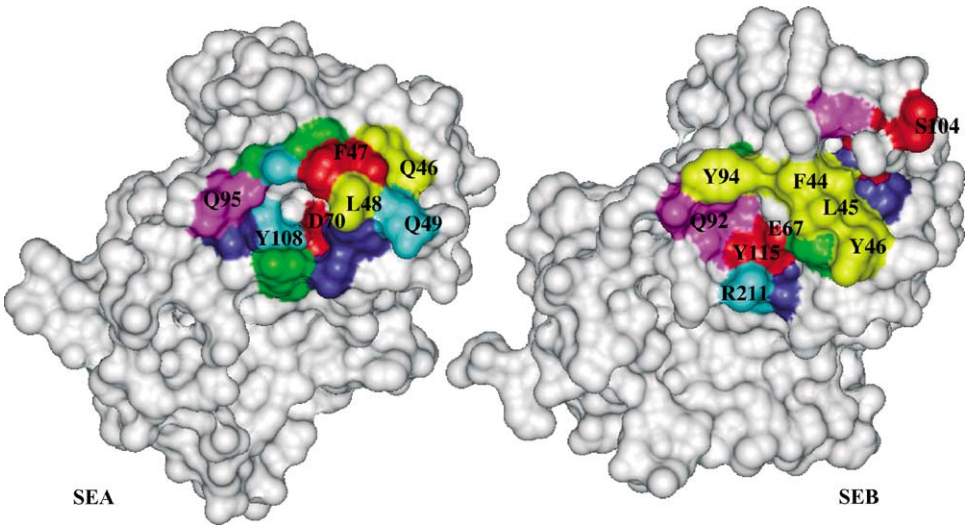

Fig. 4. Binding signatures for docked SEA and SEB complex configurations with DR1α. Shown are residue free energy contributions projected onto the molecular surfaces. The free energy scale (kcal/mol) is as follows. Color red: ΔG_{res} contribution ≤ -4 kcal/mol; yellow: ΔG_{res} contribution >-4 to ≤ -3 kcal/mol; purple: ΔG_{res} contribution >-3 to ≤ -2 kcal/mol; cyan: ΔG_{res} contribution >-2 to ≤ -1 kcal/mol; green: ΔG_{res} contribution >-1 to ≤ 0 kcal/mol; blue: ΔG_{res} contribution >0 kcal/mol.

Table 3
Computed free energies (kcal/mol) for pair-wise electrostatic interactions

Pair	ΔG_{pair}	$\Delta G^{-}_{m,ele}$	$\Delta G^{+}_{m,ele}$	$\Delta G^{-+}_{m,ele}$	$\Delta\Delta G^{-}_{s,ele}$	$\Delta\Delta G^{+}_{s,ele}$	$\Delta\Delta G^{-+}_{s,ele}$	ΔG^{-+}_{ele}
SEA interactions								
Q46–αK67	−6.3	3.2	−19.0	−22.1	1.1	17.8	18.9	−3.2
D70–αK39	−16.0	4.3	−0.2	−11.9	5.5	18.3	23.8	11.9
Y92–αK39	−1.3	0.0	−14.9	−16.2	0.5	18.3	18.8	2.6
Y108–αK39	−2.0	0.4	−14.2	−15.8	0.9	18.3	19.2	3.4
SEB interactions								
Q43–αK67	1.0	0.0	−45.0	−44.0	0.6	30.0	30.6	−13.4
E67–αK39	−38.1	7.1	−5.9	−36.9	15.1	33.8	48.9	12.0
Y89–αK39	−2.4	−1.0	−41.6	−45.0	0.5	33.8	34.3	−10.7
Y115–αK39	−7.6	0.9	−36.4	−43.1	1.3	33.8	35.1	−8.0

tyrosines in the polar pocket, each in SEB forming hydrogen bonds with DR1α_1 Lys39, while in SEA the interactions are much weaker.

3.3. Electrostatic pair interactions

Though the decomposition of the ΔG_{micro} indicates that the interactions of the SEA and SEB polar pocket stabilizes the association with DR1α, it is not clear as to what role the hydrophilic bridges (ion-pair and/or hydrogen bonds) play in the total free energy of complex formation. Table 3 shows the free energy terms for several SEA and SEB interaction pairs. The calculations reveal that while the energetics of the SEA and SEB charged residues in the polar pocket with DR1 can compensate for their individual desolvation penalties on a per-residue level (Table 2), the hydrophilic bridges in themselves contribute unfavorably to the stability of the protein–protein complexes ($\Delta G^{-+}_{ele} > 0$). The reason for this is that ion-pair interaction (ΔG_{pair}) plus the interaction of the charged residue with the rest of the complex ($\Delta G^{-+}_{m,ele}$) does not compensate for the high desolvation cost of the two charged groups forming the hydrophilic bridge ($\Delta\Delta G^{-+}_{s,ele}$). Interestingly, even though the energetics for SEB Glu67 is more favorable than that of SEA Asp70 (Table 2), the calculations show a destabilization of the SEB complex by 12.0 kcal/mol, which is comparable to 11.9 kcal/mol for the SEA complex.

For the two tyrosines in the SEA polar pocket interacting DR1α_1 Lys39, the calculations show similar results, indicating unfavorable net free energies of complex formation. By contrast, the SEB tyrosines containing hydrogen bonds make favorable contributions to the complex, leading to greater binding affinity of the α-chain.

3.4. SEA–DR1β docking

While the docking of SEA with DR1α is determined primarily by surface contact, binding of DR1β is achieved through less restrictive surface matching of the zinc-coordination site (see Fig. 1). SEA residues interacting with the zinc ion include His187, His225, and Asp227, which combine to form a small cavity. In docking DR1β, the N-terminus of SEA was truncated at the first six residues, thus opening the zinc cavity for DR1 interactions. The smaller surface complementarity of this cavity region with DR1β places difficult constraints on sampling sufficient orientational space. Significantly, of more than 8 million matches attempted, only four orientations were found to satisfy the scoring criteria. These complex configurations are illustrated in Fig. 5, with the N-terminus (residues 1–20) repositioned by using a MD simulation.

The top-scoring ΔG_{micro} for DR1β is 50.8 kcal/mol, and compared with the docking of DR1α, clearly indicates that the accuracy of the value does not permit a realistic estimate of the relative binding affinity. We attribute this to the significantly large vdW clashes between the two docking proteins, resulting in a reduction of the hydrophilic contribution of the zinc ion. As expected, the surface complementarity governing the association of DR1β versus DR1α is notably smaller (a ΔG_{cav} of −21 versus −49 kcal/mol), and the largest contribution to ΔG_{micro} is the desolvation penalty of SEA at the zinc-coordination interface. The most favorable zinc-binding mode is shown in Fig. 5b, and exhibits an angle of 106.1° for the complex SEA His225 Nε2–Zn^{2+}–DR1β His81 Nδ1. This angle is typical of a tetrahedral geometry; however, additional conformational changes involving at least one of the SEA ligands is necessary to achieve full tetrahedral zinc-coordination geometry. Based on thermal factors, the sidechain of His187 could conceivably accommodate a positional shift upon chelation by DR1β His81, consequently achieving a tetrahedral configuration common for zinc-containing metalloproteins.

Our results also show that complex formation through the zinc-binding site could be achieved without rotating the imidazole ring of DR1β His81, thus preserving the hydrogen bond between the sidechain and backbone of the antigenic peptide at P3. In addition, the N-terminus of the modeled 13-residue polyalanine peptide, contributes a small interfacial free energy to the calculated ΔG_{micro}, arising from interactions with SEA residues Trp130 and Tyr229. This result suggest, that given a bound peptide with large solvent-exposed sidechains, the association of SEA with DR1β may be peptide-dependent and affected by the polymorphism of class II MHC molecules.

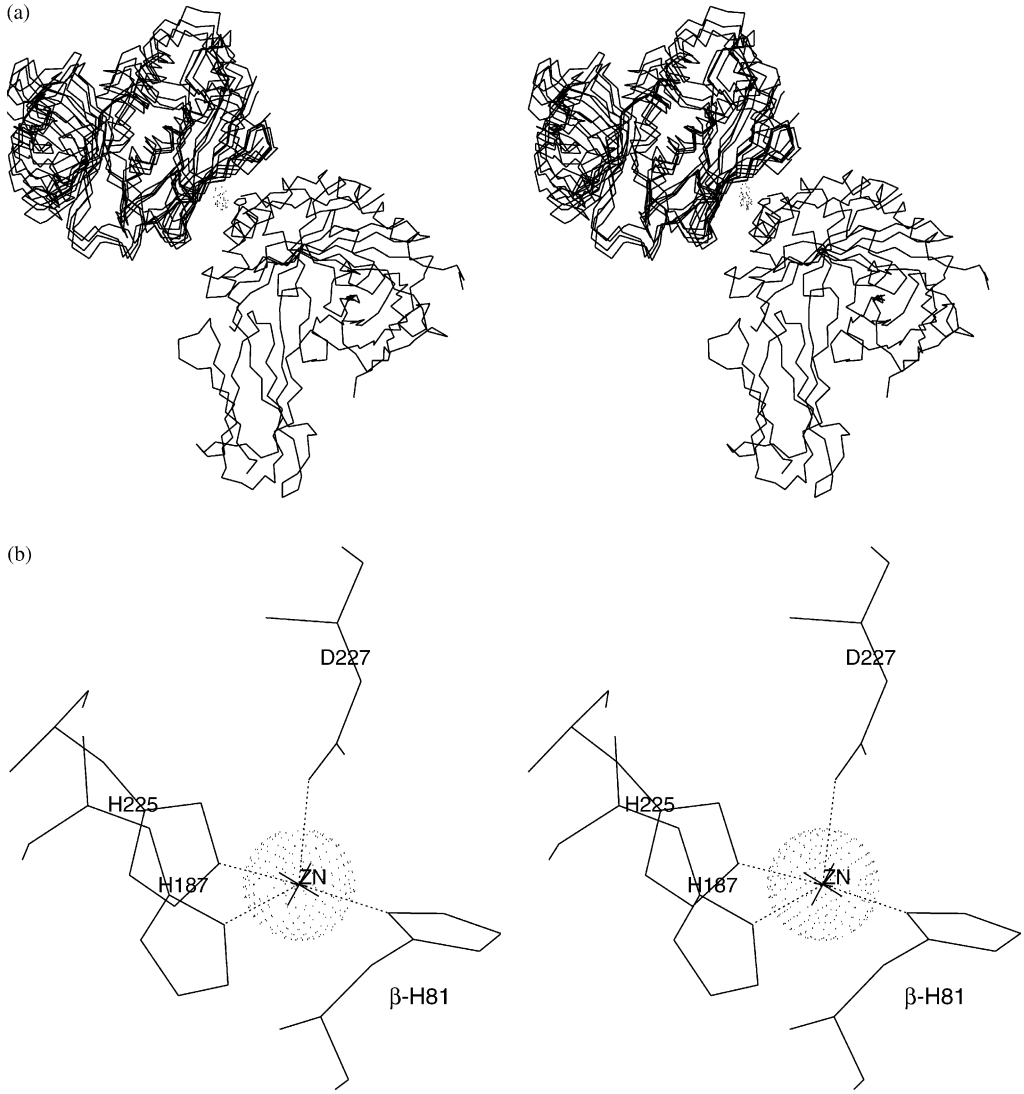

Fig. 5. (a) Stereographic illustration of generated orientations for docking SEA zinc-coordination site with DR1β. The Zn^{2+} moiety is shown as a vdW surface. (b) Local interactions of the best-scoring zinc-coordination interface between SEA and DR1β. Possible hydrophilic interactions are depicted by dashed lines.

3.5. Bivalent association and cooperativity

The predicted DR1α and DR1β-binding sites on a single HLA-DR1 molecule are sufficiently separated for simultaneous association of two SEA molecules, forming an SEA–βDRα–SEA complex (see discussion and illustrations below). Formation of the trimer is thought to be minimally a two-step process [10], initiated by the binding of SEA to the DR1β, followed by cooperative binding of a second SEA molecule to DR1α. This cooperative effect can be observed in the calculated ΔG_{micro} of the trimer by using the most favorable docked orientations for both domains. Implementing a two-step pathway of association, the ΔG_{micro} for binding the second SEA molecule is reduced by 5.7 kcal/mol, arising primarily from more favorable electrostatic interactions plus a decrease in desolvation effects of SEA upon binding DR1α. Both contributions are partially offset by an increase in the desolvation penalty for the associated SEA–DRβ state. The change in interfacial free energy is small, showing few significant surface contacts between the two SEA molecules, which may indicate weak stability for dimer formation [41]. As for the DR1β–SEA–DR1α complex, cross-linking of two HLA-DR1 molecules leads to a negligible change in the sum of individual ΔG_{micro} values from the calculated trimer ΔG_{micro}, suggesting little cooperativity at the semi-macroscopic level.

3.6. TcR–SEA–DR1 complex

While the SEA–βDrα–SEA complex has a more favorable ΔG_{micro} than the alternative DR1β–SEA–DR1α in solution, we find that this latter complex, when combined

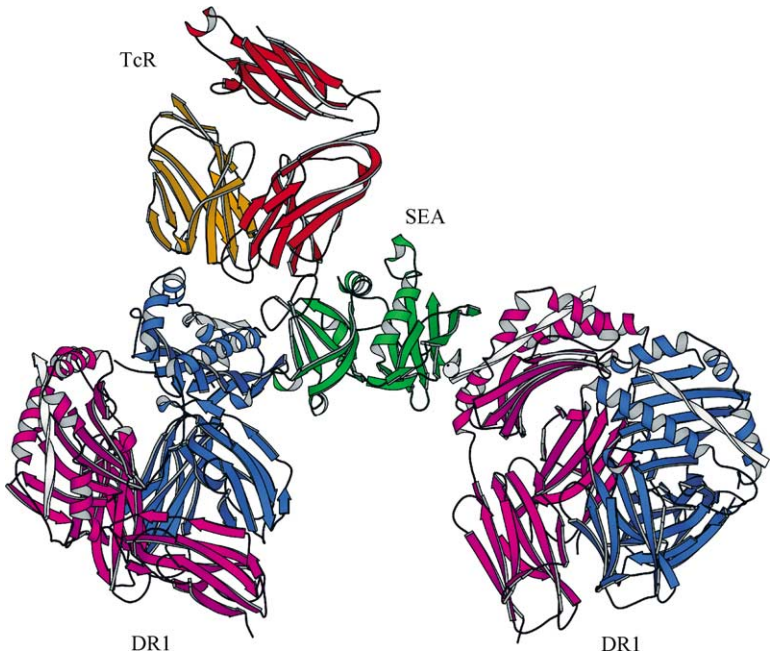

Fig. 6. Predicted TcR–(DR1β–SEA–DR1α) ternary complex. Ribbons representations shown are: SEA (green), DR1 dimer (blue and violet), antigenic peptide (white), β-chain of TcR (red), and α-chain of TcR (orange). Zinc ion is depicted by a vdW surface colored white. An association of a second SEA, interacting with the free site of DR1β, is not feasible due to being sterically inhibited by Vα of the docked TcR.

with a docked αβ-associated TcR, yields an assembly that is structurally more plausible. Fig. 6 shows a modeled ternary complex derived from the DR1β–SEA–DR1α trimer employing the most favorable docked SEA orientations for both domains. Methodology selecting the TcR orientation was similar as used with SEA, where 16 million Vβ docked conformers were generated and 135 satisfied the initial scoring criteria.

For the TcR–(SEA–βDRα–SEA) complex, SEA bound to DR1β prevents by steric hindrance with Vα the interactions between Vβ and SEA bound to DR1α. This suggests that, although observed in free solution, the stoichiometry of two SEA molecules associated with one DR1 molecule yields a non-productive SEA–DR1 complex for T-cell stimulation. The steric clash cannot be avoided by rotating the SEA molecule on the surface of DR1β, and at the same time, preserving the tetrahedral geometry of the zinc-binding mode. Moreover, displacement of the Vα domain, while retaining the interactions of Vβ with SEA, would result in a highly distorted VαVβ dimer, thus imposing an enormous energetic penalty upon complex formation. Albeit SEA and SEC lack similar Vβ specificities, we believe it would be highly unlikely that SEA–DR1 association would exhibit a Vβ conformational-binding mode drastically different from that observed in SEC3 [18]. Rotation of the complete dimer to avoid the bad clashes makes it impossible to spatially associate the complementarity determining regions (CDRs) plus the hypervariable region 4 (HV4) with SEA bound to DR1α while maintaining a second SEA positioned on DR1β.

In the case of the modeled TcR–(DR1β–SEA–DR1α) complex, the Vβ-binding sites on SEA determined from mutagenesis studies [9,42] are all solvent accessible to the docked αβ TcR. These SEA residues, interacting with CDR2 and CDR3, include Asn25, Tyr32, Arg61, Tyr64, Tyr205, Ser206, and Asn207. Possible CDR1 contacts may include Asn102 and Lys103. The Vβ domain in our model lacks any significant surface contacts with DR1, as does Vα with the surface of SEA. There are, however, stable interfacial and electrostatic free energies of interactions between Vα and DR1β. These modeled interactions support the idea of a functional interaction surface between TcR–DR1 required for favorable recognition and T-cell response to SAgs [43]. Included in the interface are residues located in the Vα CDR2, interacting with the long α-helix of DR1β. Our model also suggests, that in addition to the interactions with SEA, the HV4 is oriented over the peptide and may influence Vβ specificity.

A comparison between our modeled TcR binding with SEA and a recent reported homology model [44] of a similar complex shows significant binding differences. As noted above, our docking approach samples surface complementarity and scores the complex configurations via free energies, rather than forcing structural similarity with a known complex. A further difference is that unlike the published homology model, the Vβ sequence used in our docking study is one that interacts with SEA. A more meaningful assessment of our model can be made using recent crystallographic determinations of two streptococcal SAgs bound to TcR β-chains [45]. Despite our comparative model of the

TcR using the SEC3 cocrystal structure, docking captures a global-binding mode that is consistent with the streptococcal complexes. There is, however, an orientational displacement of Vβ approximately 0.5–6.0 Å in the bound contact loops between our model and the SpeA complex. This can be attributed to structural and sequence variability among the SAgs, which leads to diversity in the architecture of TcR signaling complexes [45].

3.7. Large-scale assembly

An important structural feature of the zinc-containing SEA is the possibility of forming unique multimeric clusters. Multimeric assembly of SEA may contribute significantly to a higher efficiency of T-cell activation than is possible for monovalent SAgs (e.g. SEB). Question is, under what structural conditions permit SEA to cross-link class II MHC molecules and αβ TcRs beyond the limited ternary complexes? Assuming the predicted assembly outlined above and applying dimerization of DR1, as observed in the SEB–DR1 cocrystal structure, we constructed a model for a multimeric complex of SEA molecules. Fig. 7 illustrates the model built from four clusters of TcR–(DR1β–SEA–DR1α) complexes.

Several important observations can be made from our model. First, assembly of SEA–DR1 complexes capable of

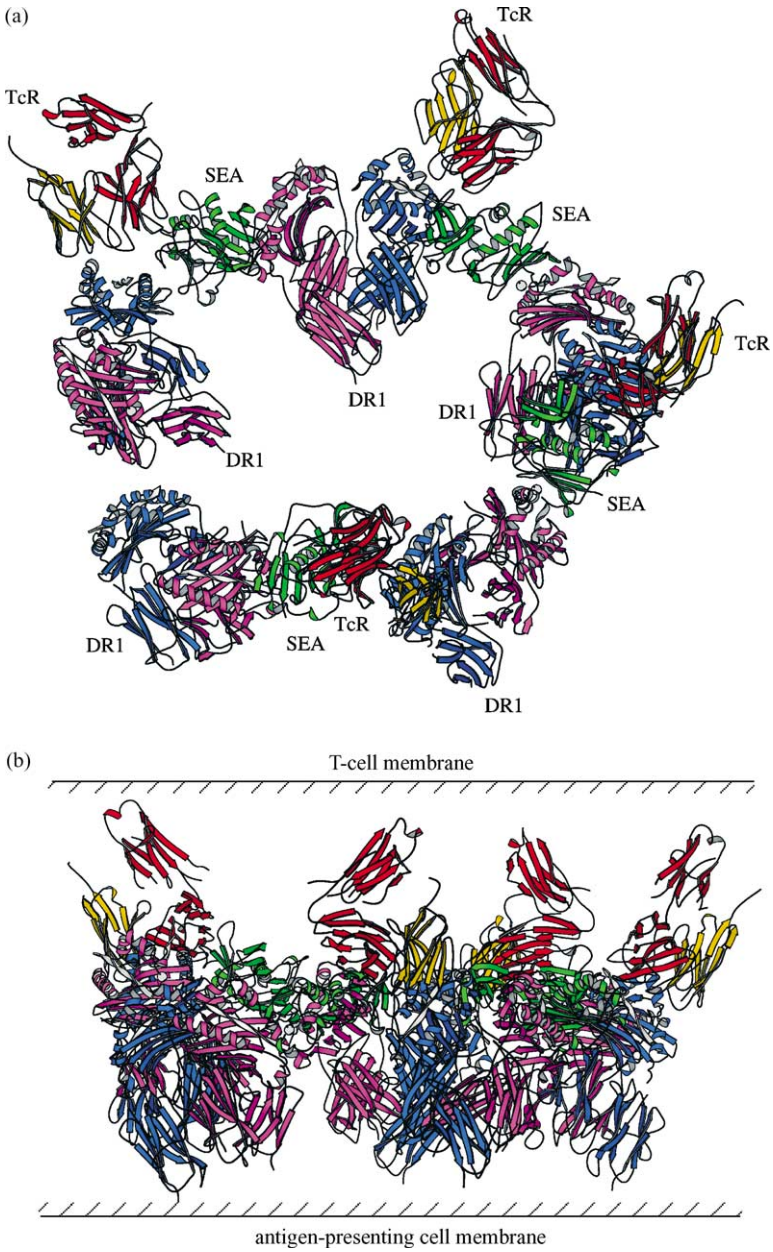

Fig. 7. (a) Model for the large-scale assembly of four TcR–(DR1β–SEA–DR1α) ternary complexes. Color scheme is similar to that used in Fig. 6. (b) Structures perpendicular to the plane of T-cell and antigen-presenting cell membranes.

engaging TcRs is constrained by the requirement for dimerization of DR1. Whether dimerization of class II MHC molecules indeed occurs on antigen-processing cells remains an open question. In constructing our structural model, the C-termini of each DR1 β-chain is oriented perpendicular to the plane of the cell membrane (Fig. 7b), which is consistent with the notion of class II MHC glycoproteins acting as molecular scaffolds for binding and presenting antigens. Similarly, the constant regions of the modeled TcRs are perpendicular to a single T-cell membrane plane. Second, the modeled assembly is limited to a finite size of either four or five ternary complex modules, with the caveat of uncertainties in the predicted rigid-body-binding modes (i.e. the gap in the circular structure of the assembly may be filled with a fifth SEA). Without the constraints of engaging TcRs, DR1 dimerization is not needed and oligomers can grow much larger, assuming a cooperative mechanism of binding SEA.

The final observation is that the dimerization or stacking of αβ TcRs, as in proposed models for T-cell activation of conventional antigens [46], is unlikely for SAgs. The modeled assembly shows that the orientation of TcRs associated with SEA molecules preclude, through steric hindrance, the dimerization of different TcRs. Moreover, no multimeric stacking of TcRs is possible between different oligomeric structures, interacting in a manner with the dimer DR1 molecules as with conventional antigens [22]. Similar inference can be made for monovalent SAgs, suggesting that TcR dimerization is not necessary for T-cell activation.

Acknowledgements

We are indebted to the late D.C. Wiley for making various crystallographic structures available throughout his outstanding career, also D.H. Ohlendorf, L.A. Svensson, and R.A. Mariuzza. We gratefully acknowledge the Biomedical Supercomputing Center of the Frederick Cancer Research and Development Center for a generous grant of computer time. The work of L.C. was supported by the AHPCRC under the auspices of the Department of the Army, Army Research Laboratory cooperative agreement number DAAH04-95-2-0003/DAAH04-95-C-0008.

References

[1] B.A. Fields, E.L. Malchiodi, H. Li, X. Ysern, C.V. Stauffacher, P.M. Schlievert, K. Karjalainen, R.A. Mariuzza, Crystal structure of T-cell receptor β-chain complexed with a superantigen, Nature 384 (1996) 188–192.

[2] E.E. Malchiodi, E. Eisenstein, B.A. Fields, D.H. Ohlendorf, P.M. Schlievert, K. Karjalainen, R.A. Mariuzza, Superantigen binding to a T cell receptor β chain of three dimensional structure, J. Exp. Med. 182 (1995) 1845–1853.

[3] R.G. Ulrich, S. Bavari, M.A. Olson, Bacterial superantigens in human disease: structure, function and diversity, Trends Microbiol. 3 (1995) 463–468.

[4] L. Abrahmsén, M. Dohlsten, S. Segrén, P. Björk, E. Jonsson, T. Kalland, Characterization of two distinct MHC class II binding sites in the superantigen staphylococcal enterotoxin A, EMBO J. 14 (1995) 2978–2986.

[5] R.E. Tiedemann, J.D. Fraser, Cross-linking of MHC class II molecules by staphylococcal enterotoxin A is essential for antigen-presenting cell and T cell activation, J. Immunol. 157 (1996) 3958–3966.

[6] E.M. Schad, I. Zaitseva, V.N. Zaitsev, M. Dohlsten, T. Kalland, P.M. Schlievert, D.H. Ohlendorf, L.A. Svensson, Crystal structure of the superantigen staphylococcal enterotoxin type A, EMBO J. 14 (1995) 3292–3301.

[7] M. Sundström, D. Hallén, A. Svensson, E. Schad, M. Dohlsten, L. Abrahmsén, The co-crystal structure staphylococcal enterotoxin type A with Zn^{2+} at 2.7 Å, J. Biol. Chem. 271 (1996) 32212–32216.

[8] T.S. Jardetzky, J.H. Brown, J.C. Gorga, L.J. Stern, R.G. Urban, Y. Chi, C. Stauffacher, J.L. Strominger, D.C. Wiley, Three-dimensional structure of a human class II histocompatibility molecule complexed with superantigen, Nature 368 (1994) 711–718.

[9] R.G. Ulrich, S. Bavari, M.A. Olson, Staphylococcal enterotoxins A and B share a common structural motif for binding class II major histocompatibility complex molecules, Nat. Struct. Biol. 2 (1995) 554–560.

[10] R.E. Tiedemann, R.G. Urban, J.L. Strominger, J.D. Fraser, Isolation of HLA-DR1·(staphylococcal enterotoxin A)$_2$ trimers in solution, Proc. Natl. Acad. Sci. U.S.A. 92 (1995) 12156–12159.

[11] J. Thibodeau, M. Dohlsten, I. Cloutier, P. Lavoie, P. Bjork, F. Michel, C. Léveillé, W. Mourad, T. Kalland, R.P. Sékaly, Molecular characterization and role in T-cell activation of staphylococcal enterotoxin A binding to the HLA-DR α-chain, J. Immunol. 10 (1997) 3698–3704.

[12] K.R. Hudson, R.E. Tiedemann, R.G. Urban, S.C. Lowe, J.L. Strominger, J.D. Fraser, Staphylococcal enterotoxin A has two cooperative binding sites on major histocompatibility complex class II, J. Exp. Med. 182 (1995) 711–720.

[13] E.C. Meng, D.A. Gschwend, J.M. Blaney, I.D. Kuntz, Orientational sampling and rigid-body minimization in molecular docking, Proteins 17 (1993) 266–278.

[14] B.K. Shoichet, I.D. Kuntz, Protein docking and complementarity, J. Mol. Biol. 221 (1991) 327–346.

[15] M.A. Olson, L. Cuff, Molecular docking of superantigens with class II major histocompatibility complex proteins, J. Mol. Recog. 10 (1997) 277–289.

[16] J. Kim, R.G. Urban, J.L. Strominger, D.C. Wiley, Toxic shock syndrome toxin-1 complexed with a class II major histocompatibility molecule HLA-DR1, Science 266 (1994) 1870–1874.

[17] B.A. Fields, E.L. Malchiodi, H. Li, X. Ysern, C.V. Stauffacher, P.M. Schlievert, K. Karjalainen, R.A. Mariuzza, Crystal structure of T-cell receptor β-chain complexed with a superantigen, Nature 384 (1996) 188–192.

[18] M.L. Connolly, Molecular Surface Program 429. The Quantum Chemistry Program Exchange, Indiana University, Bloomington, IN 47405, USA, 1981.

[19] S.J. Weiner, P.A. Kollman, D.T. Nguyen, D.A. Case, An all atom force field for simulations of proteins and nucleic acids, J. Comp. Chem. 7 (1986) 230–252.

[20] S.C. Hoops, K.W. Anderson, K.M. Merz Jr., Force field design for metalloproteins, J. Am. Chem. Soc. 113 (1991) 8262–8270.

[21] B. Arden, S.P. Clark, D. Kabelitz, T.W. Mak, Mouse T-cell receptor variable gene segment families, Immungenetics 42 (1995) 501–530.

[22] D.N. Garboczi, P. Ghosh, U. Ultz, Q.R. Fan, W.E. Biddision, D.C. Wiley, Structure of the complex between human T-cell receptor, viral peptide and HLA-A2, Nature 383 (1996) 134–141.

[23] M.A. Olson, Calculations of free energy contributions to protein–RNA complex stabilization, Biophys. J. 81 (2001) 1841–1853.

[24] R.M. Jackson, M.J.E. Sternberg, Application of scaled particle theory to model the hydrophobic effect: implications for molecular association and protein stability, Protein Eng. 7 (1994) 371–383.

[25] A. Nicholls, K.A. Sharp, B. Honig, Protein folding and association: insights from the interfacial and thermodynamic properties of hydrocarbons, Proteins 11 (1991) 281–296.
[26] M.K. Gilson, B. Honig, Calculation of the total electrostatic energy of a macromolecular system: solvation energies, binding energies, and conformational analysis, Proteins 4 (1988) 7–18.
[27] Y.Y. Sham, Z.T. Chu, H. Tao, A. Warshel, Examining methods for calculations of binding free energies: LRA, LIE, PDLD-LRA, and PDLD/S-LRA calculations of ligands binding to an HIV protease, Proteins 39 (2000) 393–407.
[28] M.A. Olson, T.L. Armendinger, Free energy contributions to complex formation between botulinuum neurotoxin type B and synaptobrevin fragment, Protein Eng. 9 (2002) 739–743.
[29] M.A. Olson, Mean-field analysis of protein–protein interactions, Biophys. Chem. 75 (1998) 115–138.
[30] Z.S. Hendsch, B. Tidor, Do salt bridges stabilize proteins? A continuum electrostatic analysis, Protein Sci. 3 (1994) 211–226.
[31] J. Janin, Quantifying biological specificity: the statistical mechanics of molecular recognition, Proteins 25 (1996) 438–445.
[32] M. Karplus, J. Janin, Comment on: the entropy cost of protein association, Protein Eng. 12 (1999) 185–186.
[33] L. Abrahmsén, Superantigen engineering, Curr. Opin. Struct. Biol. 5 (1995) 464–470.
[34] R.M. Jackson, M.J.E. Sternberg, A continuum model for protein–protein interactions: application to the docking problem, J. Mol. Biol. 250 (1995) 258–275.
[35] N. Froloff, A. Windemuth, B. Honig, On the calculation of binding free energies using continuum methods: application to MHC class I protein–peptide interactions, Protein Sci. 6 (1997) 1293–1301.
[36] G. King, F. Lee, A. Warshel, Microscopic simulations of macroscopic dielectric constants of solvated proteins, J. Chem. Phys. 95 (1991) 4366–4377.
[37] A. Warshel, J. Åqvist, Electrostatic energy and macromolecular function, Ann. Rev. Biophys. Biophys. Chem. 20 (1991) 267–298.
[38] I. Muegge, T. Schweins, A. Warshel, Electrostatic contributions to protein–protein binding affinities: application to Rap/Raf interaction, Proteins 30 (1998) 407–423.
[39] M.A. Olson, L.T. Reinke, Modeling implicit reorganization in continuum descriptions of protein–protein interactions, Proteins 38 (2000) 115–119.
[40] K. Mehindate, J. Thibodeau, M. Dohlsten, T. Kalland, R.P. Sekaly, W. Mourad, Cross-linking of major histocompatibility complex class II molecules by staphylococcal enterotoxin A superantigen is a requirement for inflammatory cytokine gene expression, J. Exp. Med. 182 (1995) 1573–1577.
[41] M. Sumdström, L. Abrahmsén, P. Antonsson, K. Mehindate, W. Mourad, M. Dohlsten, The crystal structure of staphylococcal enterotoxin type D reveals Zn^{2+}-mediated homodimerization, EMBO J. 24 (1996) 6832–6840.
[42] Y. Bravo de Alba, P.N. Marche, P.A. Cazenave, I. Cloutier, R.P. Sekaly, J. Thibodeau, Vα domain modulates the multiple topologies of mouse T cell receptor Vβ20/staphylococcal enterotoxins A and E complexes, Eur. J. Immunol. 27 (1997) 92–99.
[43] P. Antonsson, A.G. Wingren, J. Hansson, T. Kalland, M. Varga, M. Dohlsten, Functional characterization of the interaction between the superantigen staphylococcal enterotoxin A and the TcR, J. Immunol. 158 (1997) 4245–4251.
[44] H.I. Krupka, B.W. Segelke, R.G. Ulrich, S. Ringhofer, M. Knapp, B. Rupp, Structural basis for abrogated binding between staphylococcal enterotoxin A superantigen vaccine and MHC-IIα, Protein Sci. 11 (2002) 642–651.
[45] E.J. Sundberg, H. Li, A.S. Liera, J.K. McCormick, J. Tormo, P.M. Schlievert, K. Karjalainen, R.A. Mariuzza, Structures of two streptococcal superantigens bound to TCR β chains reveal diversity in the architecture of T cell signaling complexes, Structure 10 (2002) 687–699.
[46] B.A. Fields, R.A. Mariuzza, Structure and function of the T-cell receptor: insights from X-ray crystallography, Immunol. Today 17 (1996) 330–336.